Quaternary Research 81 (2014) 151–157

Contents lists available at ScienceDirect

Quaternary Research

journal homepage: www.elsevier.com/locate/yqres

Biogenic opal production changes during the Mid-Pleistocene Transition in the Bering Sea (IODP Expedition 323 Site U1343)

Sunghan Kim [a,1], Kozo Takahashi [b,c,1], Boo-Keun Khim [a,*], Yoshihiro Kanematsu [c], Hirofumi Asahi [a], Ana Christina Ravelo [d]

[a] Department of Oceanography, Pusan National University, Busan 609-735, South Korea
[b] Hokusei Gakuen University, Sapporo 004-8631, Japan
[c] Department of Earth and Planetary Sciences, Kyushu University, Fukuoka 812-8581, Japan
[d] Ocean Sciences Department, University of California, Santa Cruz, CA 95064, USA

ARTICLE INFO

Article history:
Received 6 March 2013
Available online 15 November 2013

Keywords:
Biogenic opal
Paleoproductivity
Mid-Pleistocene Transition
Orbital cycles
Bering Sea
Subarctic North Pacific

ABSTRACT

Biogenic opal content and mass accumulation rate (MAR) at IODP Expedition 323 Site U1343 were found to fluctuate consistently, generally being high under warm conditions and low under cold conditions during the last 2.4 Ma. Continuous wavelet transform analysis of the normalized biogenic opal content indicates that export production in the Bering Sea varied predominantly at 41-ka periodicity before 1.25 Ma, and shifted to 100-ka periodicity at the onset of the Mid-Pleistocene Transition (MPT; 1.25–0.7 Ma). The 100-ka cycles dominated until the Holocene. Export production in the Bering Sea decreased markedly in the Bering Sea two times during the MPT: the first occurred at the beginning of the MPT (1.25 Ma) and the second in the middle of the MPT (0.9 Ma). These decreases coincided with both increases in the relative abundance of sea-ice diatoms and decreases in the warm-water diatom species *Neodenticula seminae*, indicating that reductions in export production in the Bering Sea during the MPT were associated with climate cooling. Decreases in export production in the Bering Sea during the MPT were most likely associated with the increased influence of polar/Arctic domains on the high-latitude North Pacific.

© 2013 University of Washington. Published by Elsevier Inc. All rights reserved.

Introduction

The Mid-Pleistocene Transition (MPT) is considered the most important global climate transition since the intensification of the Northern Hemisphere Glaciation (NHG) at 3.5 to 2.5 Ma (Mudelsee and Raymo, 2005). The MPT is characterized by the emergence of high-amplitude glacial–interglacial variability with cycle durations of ~100 ka, accompanied by ice-sheet expansion without any significant change in orbital forcing (Shackleton et al., 1988; Raymo et al., 1997; Clark et al., 2006). Although the reported timing of the MPT differed at various regions, Clark et al. (2006) proposed that the MPT spanned from 1.25 Ma to 0.7 Ma based on the global benthic oxygen isotope stack (LR-04: Lisiecki and Raymo, 2005).

Alkenone sea-surface temperatures (SSTs) decreased during the MPT at Site 846 (3°05′S, 90°49′W, 3296 m) and Site 849 (0°11′N, 110°31′W, 3851 m) in the eastern equatorial Pacific (Liu and Herbert, 2004; McClymont and Rossel-Mele, 2005) and at Site 1077 (5°10′S, 10°26′E, 2382 m) in the eastern tropical Atlantic (Schefus et al., 2004). Shallow marine sediments in Japan recorded sea levels 20–30 m lower during Marine Isotope Stage 22 (MIS 22) at ~0.9 Ma than during MIS 28 (Kitamura and Kawagoe, 2006). These results support the hypothesis that ice-sheet expansion associated with climate cooling occurred during the MPT. Based on the measurements of $\%C_{37:4}$, a proxy for subarctic/subpolar water mass distribution, at Site 983 (60°24′N, 23°38′W, 1985 m) in the northern North Atlantic and at Site 882 (50°22′N, 167°36′E, 3244 m; Fig. 1) in the northwestern North Pacific, McClymont et al. (2008) suggested that polar/Arctic water masses expanded toward the equator during the MPT. Despite these pieces of clear evidence for the climate cooling and ice-volume increases during the MPT, there have been few studies at high-latitude locations where climate changes are directly linked to cryospheric processes.

The Bering Sea is located in the northern high latitudes where seasonal sea ice forms. In particular, the Beringian slope area in the Bering Sea is influenced not only by the relatively warm subarctic water masses (the Alaskan Stream) but also by the seasonal sea-ice cover. The slope area is also characterized by high surface-water productivity (e.g., Springer et al., 1996) and high sedimentation rates (>25 cm/ka) (Expedition 323 Scientists, 2009; Itaki et al., 2009; Kim et al., 2011). Surface-water productivity in the slope area is restricted by extensive sea-ice conditions and facilitated by the input of the Bering Slope Current (BSC) (Nakatsuka et al., 1995; Clement et al., 2005; Okazaki et al., 2005), an extension of the Alaskan Stream. Nutrient supply from the subsurface layer is associated with the BSC (Okkonen

* Corresponding author.
E-mail address: bkkhim@pusan.ac.kr (B.-K. Khim).
[1] Equally-contributing author.

0033-5894/$ – see front matter © 2013 University of Washington. Published by Elsevier Inc. All rights reserved.
http://dx.doi.org/10.1016/j.yqres.2013.10.001

https://doi.org/10.1016/j.yqres.2013.10.001 Published online by Cambridge University Press

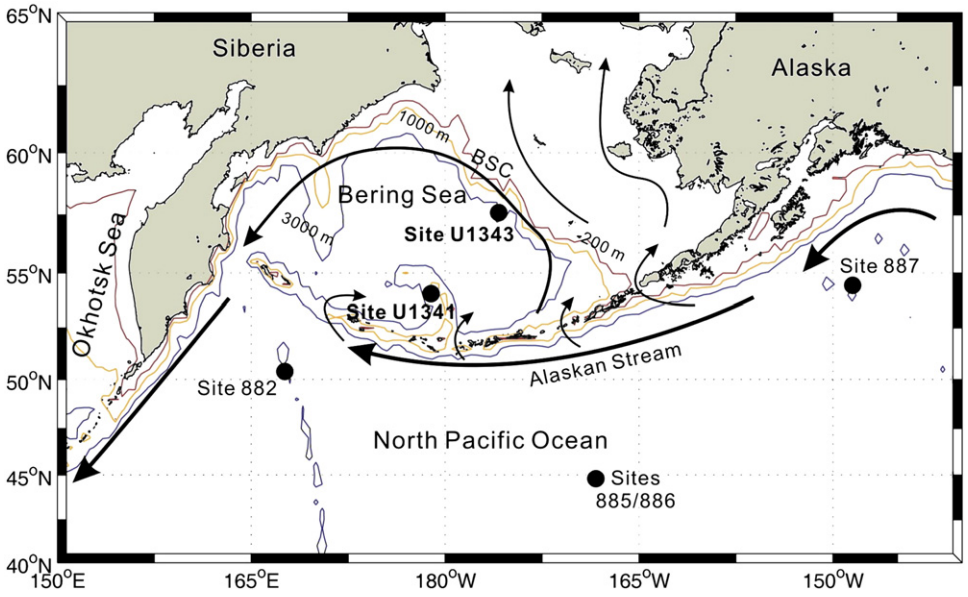

Figure 1. Schematic bathymetry of the Bering Sea and the subarctic North Pacific, illustrating the drilling locations including Site U1343. Arrows show the direction of major surface currents. The Bering Slope Current is labeled as BSC.

et al., 2004) together with tidal mixing which brings continental shelf water into the slope area (Springer et al., 1996). Thus, changes in surface-water productivity in the slope area of the Bering Sea provide crucial information regarding climate changes in the northern high latitudes during the MPT.

Export production significantly decreased during the intensification of the NHG, but was relatively low and constant through the MPT, at Site 882 in the northwestern subarctic North Pacific and at Sites 885/886 (44°41′N, 168°16′W, 5700 m; 44°41′N, 168°14′W, 5700 m, respectively; Fig. 1) in the central subarctic North Pacific (e.g., Haug et al., 1995; Snoeckx et al., 1995). However, the response of surface-water productivity to climate cooling during the MPT in the high-latitude North Pacific has not yet been determined. In this study, we reconstructed surface-water productivity variations using continuous wavelet transform analysis of the biogenic opal content and mass accumulation rate (MAR) at IODP Expedition 323 Site U1343 in the Bering Sea. Our results reveal paleoceanographic/paleoclimatic changes of the high-latitude North Pacific during the MPT.

Materials and methods

Site U1343 (57°33′N, 175°49′E, 1950 m; Fig. 1) was drilled with five holes (Sites U1343A through U1343E). A total of 1187 sediment samples from the following four holes were used in this study: Holes U1343A (205 samples from 20 to 200 m below sea floor (m bsf)), U1343C (237 samples from 0 to 235 m bsf), and U1343E (51 samples from 0 to 140 m bsf and 694 samples from 185 to 745 m bsf). The Site U1343 sediments are primarily composed of silt with varying amounts of clay and diatoms and minor amounts of sand, ash, foraminifers, calcareous nannofossils, and sponge spicules (Expedition 323 Scientists, 2009). In order to exclude the effects of core expansion and incomplete core recovery, all sediment depths are reported as the corrected core composite depth below seafloor (CCSF).

According to the sampling policy of IODP Exp. 323, Kanematsu et al. (2013) and Kim et al. (2010) undertook the biogenic opal analyses for the upper half (0–330 m bsf) and for the lower half (320–745 m bsf), respectively, at Site U1343. Kanematsu et al. (2013) compared the biogenic opal data between Site U1343 (the Bering Slope area) and Site U1341 (Bowers Ridge) and came to the conclusion that the biogenic opal contents at Bowers Ridge were significantly higher than those at the Bering Slope area. Such difference is primarily attributed to the fact that the sediments at Site U1343 were more diluted by lithogenic matter derived from the Alaskan continent as well as being more affected by sea-ice cover than those at Site U1341. Kim et al. (2010) reported that biogenic opal content and its MAR show the obvious orbital-scale glacial–interglacial variations from Late Pliocene to early Pleistocene at Site U1343. Distinct decrease of these properties occurred from 2.02 Ma to 1.8 Ma, when overall $\delta^{15}N$ values increased by nearly 2‰, which marks a transition toward low concentrations of nutrients in surface water after 1.8 Ma, leading to depressed export production and high $\delta^{15}N$ values.

This study compiles all biogenic opal data of Site U1343, although the above mentioned studies reported part of the data. However, this study is an exclusive synthesis using all biogenic opal data at Site U1343, focusing on the independent and totally different theme from those of the other studies. Here we first reveal the MPT in the Bering Sea in terms of export production based on the biogenic opal data.

Age model of Site U1343

In order to constrain the age model for Site U1343, a benthic foraminiferal oxygen isotope stratigraphy was used in this study (Fig. 2). Detailed age model construction is presented in Asahi et al. (2011). The established oxygen isotope stratigraphy of Site U1343 is mostly consistent with biostratigraphic datums and isochron ages reported in Takahashi et al. (2011) (Table 1, Fig. 2). The benthic oxygen isotope record is based on a sampling interval above 365 m CCSF of ~2 ka, whereas in the interval below 365 m CCSF it is ~11 ka. In general, sedimentation rates were high before the MPT and low after the MPT, with an average sedimentation rate of ~33 cm/ka (Fig. 2).

In order to avoid distortions in the continuous wavelet transform analysis, presumably caused by inaccurate ages of Site U1343 resulting from low-resolution oxygen isotope measurements, the ages below 370 m CCSF were recalculated by correlating very high-resolution natural gamma ray (NGR) values (Expedition 323 Scientists, 2009) with the LR-04 stack (Lisiecki and Raymo, 2005) because there is a strong relationship between NGR and benthic foraminiferal oxygen isotope values at Site U1343 (Asahi et al., 2011).

https://doi.org/10.1016/j.yqres.2013.10.001 Published online by Cambridge University Press

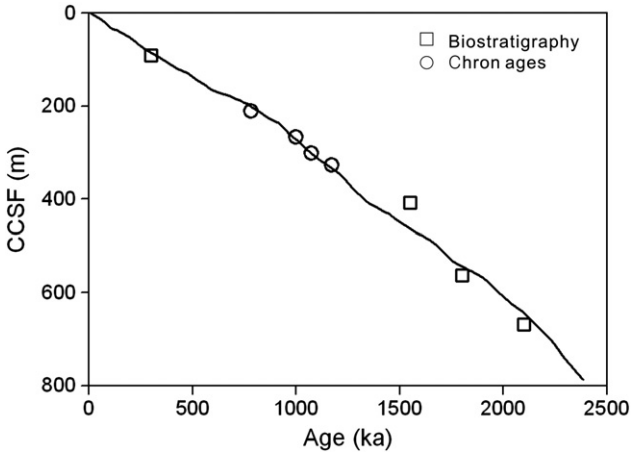

Figure 2. Age model for Site U1343 (adopted from Asahi et al., 2011). Circles and squares represent biostratigraphy and isochron ages summarized in Table 1 (Takahashi et al., 2011).

Biogenic opal content and MAR

Biogenic silica (Si_{BIO}) content was measured in 1187 sediment samples (~2-ka resolution) using a wet alkaline extraction method modified from DeMaster (1981) at Kyushu University (Japan) and Pusan National University (Korea). The relative error of Si_{BIO} content in sediment samples is less than ± 1%. The biogenic opal content was calculated by multiplying the Si_{BIO} content by 2.4 (Mortlock and Rroelich, 1989). No inter-laboratory offset correction was needed because the biogenic opal content measured at the two laboratories for identical samples were within the analytical error.

Mass accumulation rate (MAR) for biogenic opal was calculated as follows:

Biogenic opal MAR ($g/cm^2/ka$) = biogenic opal proportion × DBD (dry bulk density) (g/cm^3) × LSR (linear sedimentation rate) (cm/ka). DBD was measured onboard at approximately 3-m intervals and linear interpolation between measurements was used to obtain a DBD value for each of our samples rather than calculating from correlation between GRA density and DBD due to low correlation. Based on the age-depth information for each MIS boundary, derived from the oxygen isotope stratigraphy (Asahi et al., 2011), LSR for each MIS was calculated, and then applied for the MAR calculation.

Continuous wavelet transform analysis

In order to minimize the effect of noise, the data set was converted to a 3-point running average of biogenic opal content. For high-resolution intervals (0–160 m CCSF (0–565 ka) and 213–350 m CCSF (825–1220 ka)), a 5-point running average was used to effectively minimize the high-frequency noise. Intervals above 370 m CCSF (~1250-ka) and below 370-m CCSF are characterized by low amplitudes and high amplitudes, respectively. The variability of the variance of biogenic opal content is shown in Figure 3a. Thus, after applying the running average for smoothing, the data set was separated into two sections, one above 370 m CCSF and the other below, and each section was normalized by its mean value and standard deviation. This ensured that the amplitudes were similarly consistent throughout the core. After interpolating the normalized biogenic opal data into every 1-ka interval, continuous wavelet transform analysis was conducted using the software provided by A. Grinsted (http://www.pol.ac.uk/home/research/waveletcoherence/).

Table 1
Biostratigraphic datums and chron ages of Site U1343 (Takahashi et al., 2011).

Age (Ma)	CCSF (m)	Control point
0.3	87.3	Average depth of LO *Spongodiscus* sp.
0.781	208.0	Average depth of Brunhes bottom
0.998	267.6	Jaramillo top
1.072	302.0	Jaramillo bottom
1.173	327.1	Cobb Mountain top
1.55	407.7	LO *Filisphaera filifera*
1.8	563.4	LO *Pyxidicula horridus*
2.1	669.0	LCO *Neodenticula koizumii*

Note: LO = last occurrence, LCO = last common occurrence.

Results

Over the duration of the 2.4 Ma record, the biogenic opal content varies from 2% to 45% (Fig. 3a) and biogenic opal MAR ranges from 0.2 $g/cm^2/ka$ to 35.1 $g/cm^2/ka$ (Fig. 4a). Biogenic opal content and MAR are closely related to LR-04 stack with high values during interglacials and low values during glacials. Before 1.25 Ma, the average and standard deviation of biogenic opal content (and MAR) during the interglacial and glacial periods are 18.7 ± 8.2% (8.3 ± 4.9 $g/cm^2/ka$) and 14.3 ± 6.7% (6.7 ± 4.1 $g/cm^2/ka$), respectively. After 1.25 Ma, those of biogenic opal content (and MAR) during the interglacial and glacial periods are 10.4 ± 3.9% (4.2 ± 2.1 $g/cm^2/ka$) and 7.9 ± 3.2% (2.7 ± 1.6 $g/cm^2/ka$), respectively. Compared to after 1.25 Ma, the biogenic opal records show higher values and higher amplitude variability before 1.25 Ma, prior to the MPT (Fig. 3a). The peaks and valleys of biogenic opal content and MAR drop at 1.25 Ma, followed by a second decrease at 0.9 Ma that includes a decrease in the amplitudes, particularly for the biogenic opal MAR. The decreases in biogenic opal MAR during the MPT do not correspond to decreases in LSR (Asahi et al., 2011), suggesting that MAR values are not primarily controlled by changes in sedimentation rate (Fig. 4c).

Continuous wavelet transform of normalized biogenic opal content for Site U1343 (Fig. 3b) indicates that, in general, ~41-ka cycles (obliquity) were dominant before 1.25 Ma. At ~1.25 Ma, a 100-ka cycle (eccentricity) emerged (Fig. 3b). Although the ~100-ka cycle is not positioned within the 95% confidence contour from ~0.9 Ma to 0.6 Ma, when the biogenic opal content amplitudes decreased, the 100-ka cycle seems to be dominant after 1.25 Ma.

Discussion

Emergence of 100-ka cycle in export production during the MPT

The MPT is characterized by the emergence of 100-ka glacial–interglacial cycles. The shift from 41-ka to 100-ka periodicity during the MPT has been observed in many prior paleoceanographic proxy records, such as the benthic foraminifera oxygen isotope (Lisiecki and Raymo, 2005), alkenone SSTs (e.g., Liu and Herbert, 2004; Schefus et al., 2004; de Garidel-Thoron et al., 2005; McClymont and Rossel-Mele, 2005; Crundwell et al., 2008), and calcareous nannofossil assemblages (e.g., Marino et al., 2008). However, the parallel transition in surface-water productivity has not previously been reported. Because surface-water productivity of the Bering Sea is strongly linked to climatic forcing, it is expected that the biogenic opal record of Site U1343 will elucidate the evolution of orbital climate cycles in the high-latitude North Pacific through the MPT.

According to previous studies of the last 60 ka in the Bering Sea, export production was high during the Holocene (i.e., interglacial) and deglacial period, and low during the last glacial period (e.g., Nakatsuka et al., 1995; Okazaki et al., 2005; Brunelle et al., 2007; Caissie et al., 2010; Kim et al., 2011). The pattern of variations in biogenic opal content at Site U1343 seem to parallel global climate changes represented in LR-04 stack, confirming that there was high export production during warm conditions and low export production during cold conditions. It is also notable that the dominant periodicity for biogenic opal content clearly shifted from 41-ka to 100-ka periodicity at 1.25 Ma (Fig. 3b). The 100-ka periodicity was dominant after the MPT, especially from

https://doi.org/10.1016/j.yqres.2013.10.001 Published online by Cambridge University Press

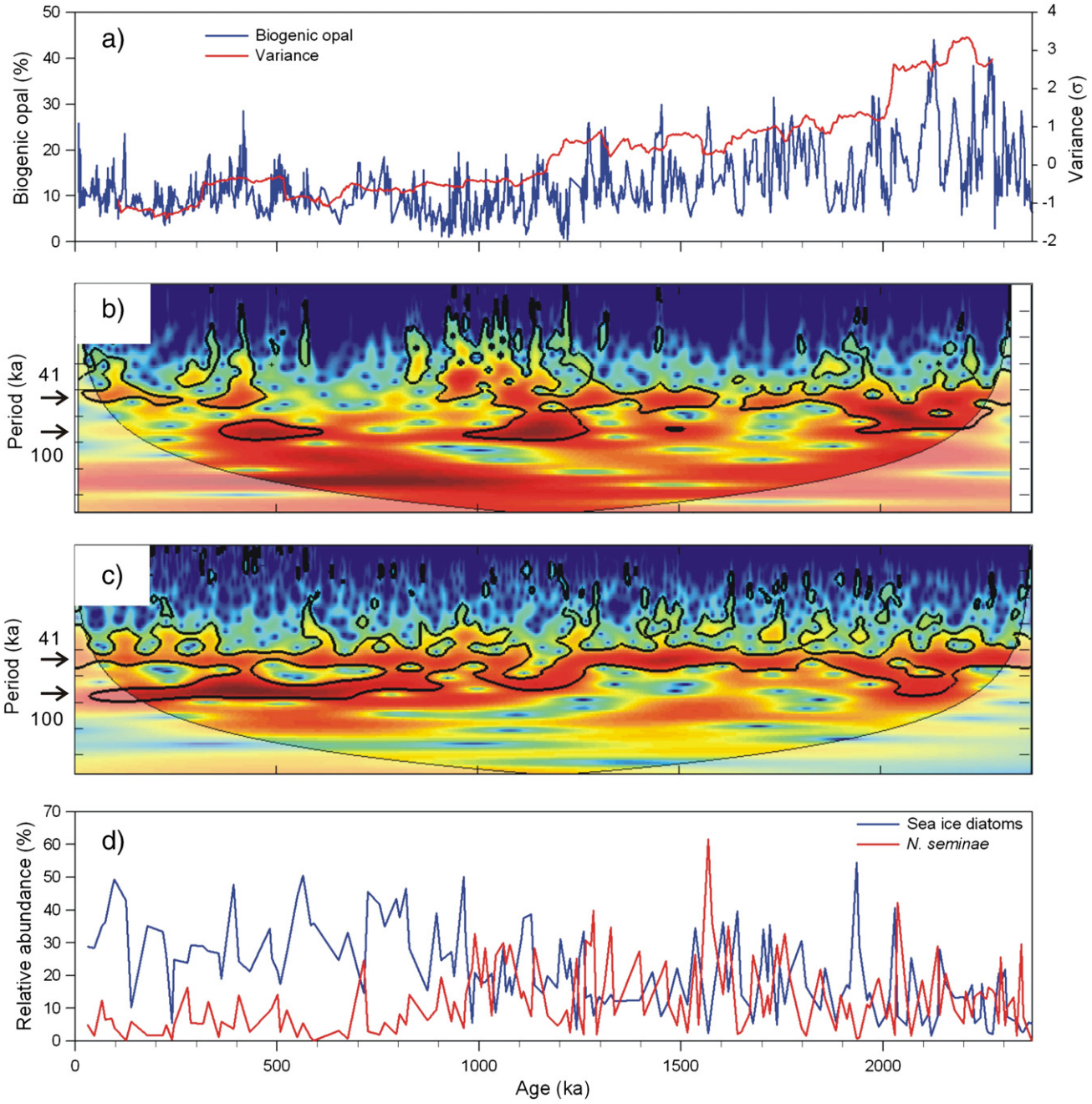

Figure 3. (a) Downcore profile of biogenic opal content and normalized variance of biogenic opal content computed in 200-ka windows with a number of lags equal to half the time series length (1/2 lags) at Site U1343, (b) continuous wavelet transform of normalized biogenic opal content at Site U1343, (c) continuous wavelet transform of the detrended LR-04 stack, and (d) downcore profile of the relative abundance of sea-ice diatoms and *Neodenticula seminae* at Site U1343 (modified from Teraishi et al., in press). Redder colors represent stronger cycles and solid lines indicate the 95% confidence levels in (b) and (c).

1.25 Ma to 0.4 Ma, although during the periods from 0.9 Ma to 0.6 Ma the cycle was not positioned within the 95% confidence line. The 41-ka cycle was also not strong during this period. The lack of significant orbital variability during this period may be attributed to low sample resolution (~6.3 ka) and/or smaller observed amplitudes (see Fig. 3a). The continuous wavelet transform of biogenic opal content at Site U1343 is similar to that of the detrended LR-04 stack calculated by Imbrie et al. (2011) (Fig. 3c). This suggests that there is an in-phased relationship between export production changes in the Bering Sea and the strengthening of polar/Arctic influences associated with global climate changes. This is manifested by the emergence of the 100-ka cyclicity in export production at Site U1343 in the Bering Sea at the beginning of the MPT (1.25 Ma).

Paleoceanographic/paleoclimatic conditions in the Bering Sea during the MPT

In the modern ocean, surface-water productivity in the Bering Sea is high under relatively warm open ocean conditions without sea ice (e.g., Sorokin, 1999). Under open ocean conditions, the slope area of the Bering Sea experiences enhanced surface-water productivity when the BSC supplies new nutrients to the area (Okkonen et al., 2004), and reduced productivity when sea ice restricts nutrient delivery (Clement et al., 2005). Thus, both biogenic opal content and MAR are likely related to the degree of surface-water biological productivity under interglacial open ocean conditions in the Bering Sea, as deduced by the close relationship between records of the biogenic opal content and the

https://doi.org/10.1016/j.yqres.2013.10.001 Published online by Cambridge University Press

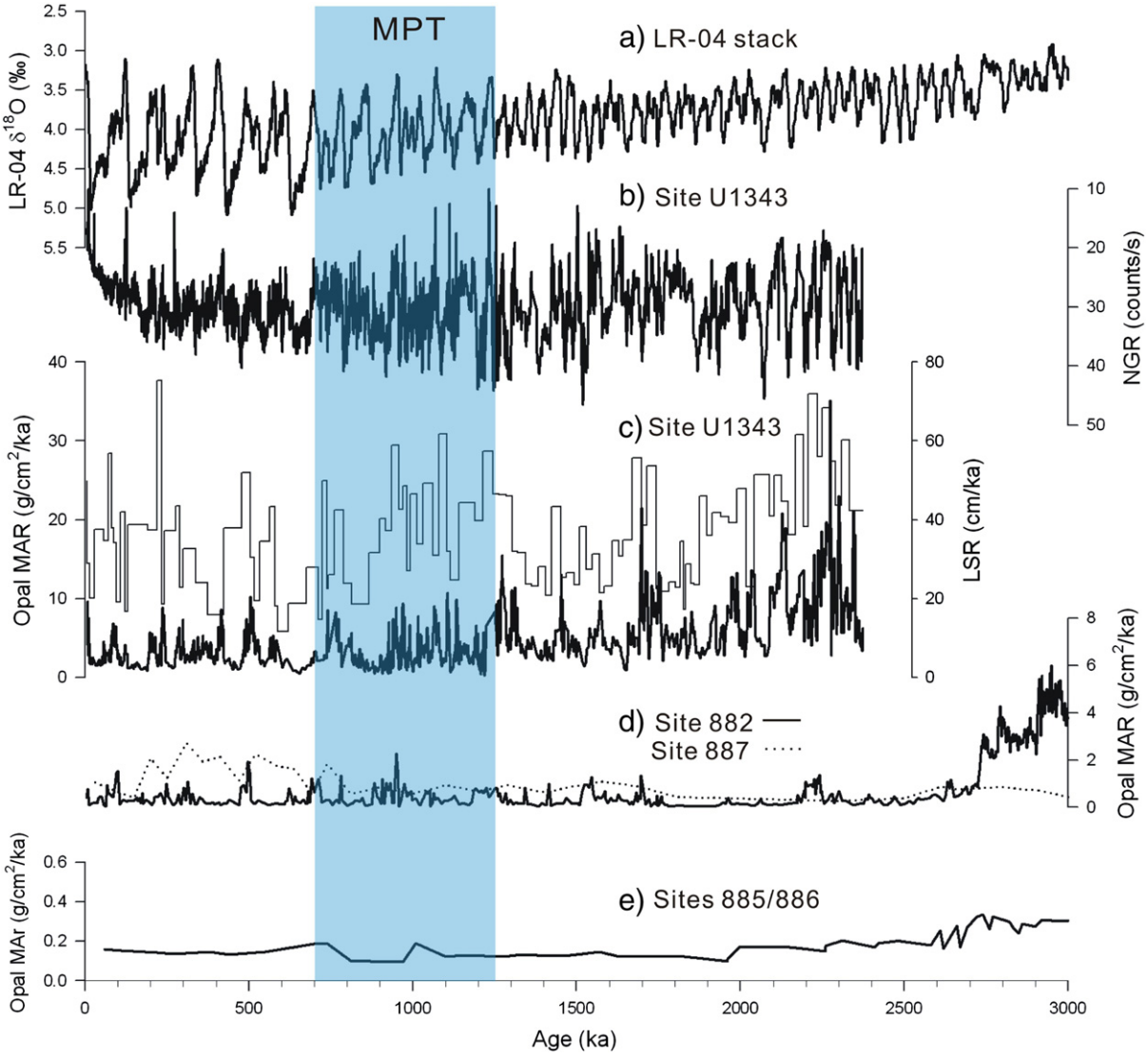

Figure 4. (a) LR-04 stack (Lisiecki and Raymo, 2005), (b) natural gamma ray (NGR) of Site U1343, (c) biogenic opal MAR and linear sedimentation rate (LSR) of Site U1343, (d) biogenic opal MAR of Site 882 in the northwestern Pacific (Haug et al., 1995) and Site 887 in the northeastern North Pacific (Rea and Snoeckx, 1995), and (e) biogenic opal MAR of Sites 885/886 in the central North Pacific (Snoeckx et al., 1995).

LR04 benthic $\delta^{18}O$ stack described in the previous section. For example, the amplitude of biogenic opal MAR variability, which reflects variations of export production between interglacial and glacial periods, was large before the MPT (Figs. 3a and 4a). Such large variations indicate that export production during warmer interglacial periods prior to the MPT under less sea ice and stronger influence of the BSC was enhanced relative to the period after the MPT, when interglacials may have been cooler and therefore more heavily influenced by sea ice and less influenced by the BSC.

Biogenic opal content shows the decreasing trend in both high and low values at 1.25 Ma compared to that before the MPT (Fig. 3a). This result indicates that export production under both warm and cold conditions decreased at the beginning of the MPT. This is supported by higher average biogenic opal MAR values in interglacial (8.3 g/cm^2/ka) and glacial (6.7 g/cm^2/ka) periods before the MPT compared to those (4.2 g/cm^2/ka and 2.7 g/cm^2/ka) after the MPT. At around 1.25 Ma, the relative abundance of sea-ice diatoms increased, whereas the relative abundance of *Neodenticula seminae*, indicative of the Alaskan Stream input, decreased (Fig. 3d; Teraishi et al., in press). Therefore, decreases in export production at the beginning of the MPT may be related to climate cooling characterized by increases in sea-ice distribution in the Bering Sea during interglacial and glacial periods. Biogenic opal MAR significantly decreased again at ~0.9 Ma, which also coincided with a major increase in the relative abundance of sea-ice diatoms and a notable decrease in the relative abundance of *N. seminae* (Figs. 3d and 4a). The amplitude of biogenic opal MAR variability became relatively small after ~0.9 Ma (Fig. 4a). This could be related to more extensive sea-ice development after ~0.9 Ma; productivity even during interglacials was relatively low compared to prior to the MPT when the climate was generally warmer and open ocean conditions prevailed. In addition, Iwasaki et al. (2011) reported that export production started to decrease at ~0.85 Ma synchronously with increases in sea-ice diatoms at Site U1341 (54°2′N, 179°0.5′E, 2140 m; Fig. 1) in the southern part of the Bering Sea. Interglacial export production during the MPT decreased without a significant change in LR-04 interglacial values, which indicate that sea-ice expansion was most likely a main trigger for global climate cooling.

In many regions, pieces of evidence regarding cooling during the MPT have been reported: decreases in alkenone SSTs (e.g., Liu and Herbert, 2004; Schefus et al., 2004; McClymont and Rossel-Mele, 2005), sea-level fall in Japan (Kitamura and Kawagoe, 2006), and increases in polar/Arctic influences at northern high latitudes (McClymont

https://doi.org/10.1016/j.yqres.2013.10.001 Published online by Cambridge University Press

et al., 2008). Because diminished export production at Site U1343 coincided with the sea-ice expansion and the reduction of warm water influences, it can be regarded as evidence for the strengthening of polar/Arctic influence as the climate cooled. Thus, the paleoceanographic/paleoclimatic conditions in the Bering Sea during the MPT have evolved in the context of global climate cooling.

Export production in the subarctic North Pacific during the MPT

Export production decreased during the NHG in the northwestern and central subarctic North Pacific (Figs. 4b and c; Haug et al., 1995; Snoeckx et al., 1995). Haug et al. (1999) proposed that surface-water stratification associated with climate cooling was the main cause for the reduction in export production in the northwestern North Pacific during the NHG. While it has been shown that northwestern North Pacific Site 882 had lower alkenone SSTs and increased polar/Arctic water mass influences during the MPT (McClymont et al., 2008; Martinez-Garcia et al., 2010), it appears that at Site 882 and at Sites 885/6 export production was more or less constant after the NHG, including the MPT, due to surface-water stratification (Figs. 4b and c; Haug et al., 1995; Snoeckx et al., 1995; Haug et al., 1999). This indicates that changes in the export production in response to climate cooling were not obvious because of strengthened surface-water stratification in the northwestern and central subarctic North Pacific.

At northeastern subarctic Pacific Site 887, however, export production increased at 0.85 Ma, which is 0.05 Ma later than the second cooling at 0.9 Ma in the Bering Sea (Fig. 4d; Rea and Snoeckx, 1995). In the modern ocean, the northeastern subarctic Pacific is known as a high-nutrient but low-chlorophyll area (Stabeno et al., 2004), and the degree of export production is most likely restricted by micronutrients such as iron (Boyd et al., 2004; Tsuda et al., 2005). The input of terrigenous material, delivered as eolian material and/or ice rafted debris (IRD), started to increase at 1.0 Ma at Site 887 in the northeastern North Pacific (Rea and Snoeckx, 1995; St. John and Krissek, 1999), accompanied by an increase in the amplitude of oxygen isotope values of benthic foraminifera at Site 677 (Shackleton and Hall, 1989). This indicates that export production was enhanced in the northeastern subarctic Pacific under climate cooling conditions, possibly due to elevated input of terrigenous materials.

The subarctic North Pacific and Bering Sea were strongly influenced by cooling climates during the MPT, as evidenced by decreasing alkenone SSTs (e.g., Martinez-Garcia et al., 2010), increasing $\%C_{37:4}$ (e.g., McClymont et al., 2008), increasing terrigenous particles and IRD (e.g., Rea and Snoeckx, 1995; St. John and Krissek, 1999), increasing sea-ice diatoms (e.g., Teraishi et al., in press), and decreasing warm water diatom species (e.g., Teraishi et al., in press). In all, these lines of evidence indicate that climate cooling during the MPT was related to the strengthening of polar/Arctic influences on the high-latitude North Pacific. Export production in the northwestern and central subarctic North Pacific was invariably constant during the MPT because of the strong surface-water stratification present after the NHG (Haug et al., 1999). In contrast, export production in the northeastern North Pacific increased during the MPT, possibly due to iron input via eolian or IRD depositional processes. In the case of the Bering Sea, the export production decreased because of a combination of extensive sea-ice formation and weakening of the warm BSC during the MPT. Our results suggest that the response of export production was regionally distinct, even under generally cooling climate conditions in the high-latitude North Pacific.

Conclusions

In this study of the last 2.4 Ma of global climate cooling, biogenic opal content and biogenic opal MAR at Site U1343, recovered from the slope area of the Bering Sea, were measured to reconstruct paleoceanographic/paleoclimatic changes during the MPT. Based on the continuous wavelet transform analysis of the normalized biogenic opal content at Site U1343, changes in the dominant cycles of export production over the last 2.4 Ma were obtained. The main points of this study are as follows:

1. Export production as represented by biogenic opal content and MAR in the Bering Sea was high during warm conditions and low during cold conditions. Export production differences between interglacial and glacial periods were much more distinct and of higher amplitude before the MPT than after the MPT.
2. Export production records in the Bering Sea clearly show a shift of dominant cycles from 41 ka to 100 ka at the beginning of the MPT (1.25 Ma).
3. The cooling transition during the MPT was characterized by two cooling periods: one at the beginning of the MPT (1.25 Ma) and a second period in the middle of the MPT (~0.9 Ma).
4. Decreasing export production during the MPT was accompanied by sea-ice expansion and weakening of the warm-water influence in the Bering Sea, which was most likely a result of climate cooling caused by the enhancement of polar/Arctic influences at high latitudes. This decrease in productivity during the MPT differs from the lack of productivity in the northwestern and central North Pacific and from the increase in productivity in the northeastern North Pacific, demonstrating that there are strong regional differences in the biological response to cooling climate and ocean conditions.
5. Climate cooling during the MPT is evident across the subarctic North Pacific and the Bering Sea. In the high-latitude North Pacific, cooling during the MPT was likely a result of increased polar/Arctic influences.

Acknowledgments

We would like to thank the crew and all onboard scientists of IODP Expedition 323, July–September 2009, and everyone in the core sampling parties for their assistance in core sampling which took place during November–December 2009 and March 2010 at Kochi Core Center, Kochi University/JAMSTEC. We appreciate editor (Tom Marchitto) and two anonymous reviewers for their constructive comments and suggestion for the improvement of the manuscript. This research was supported by the Center for Atmospheric Sciences and Earthquake Research (Grant No. CATER 2012-7040 to BKK).

References

Asahi, H., Kender, S., Ikehara, M., Sakamoto, T., Ravelo, A.C., Alvarez Zarikian, C.A., Takahashi, K., 2011. Foraminiferal oxygen isotope records at the Bering slope (IODP Exp. 323 Site U1343) provide an orbital scale age model and indicate pronounced changes during the Mid-Pleistocene Transition. American Geophysical Union, Fall Meeting, abstract #PP31B-1870.

Boyd, P.W., Law, C.S., Wong, C.S., Nojiri, Y., Tsuda, A., Levasseur, M., Takeda, S., Rivkin, R., Harrison, P.J., Strzepek, R., Gower, J., McKay, R.M., Abraham, E., Arychuk, M., Barwell-Clarke, J., Crawford, W., Crawford, D., Hale, M., Harada, K., Johnson, K., Kiyosawa, H., Kudo, I., Marchetti, A., Miller, W., Needoba, J., Nishioka, J., Ogawa, H., Page, J., Robert, M., Saito, H., Sastri, A., Sherry, N., Soutar, T., Sutherland, N., Taira, Y., Whitney, F., Wong, S.K.E., Yoshimura, T., 2004. The decline and fate of an iron-induced subarctic phytoplankton bloom. Nature 428, 549–553. http://dx.doi.org/10.1038/nature02437.

Brunelle, B.G., Sigman, D.M., Cook, M.S., Keigwin, L.D., Haug, G.H., Plessen, B., Schettler, G., Jaccard, S.L., 2007. Evidence from diatom-bound nitrogen isotopes for subarctic Pacific stratification during the last ice age and a link to North Pacific denitrification changes. Paleoceanography 22, PA1215. http://dx.doi.org/10.1029/2005PA001205.

Caissie, B.E., Brigham-Grette, J., Lawrence, K.T., Herbert, T.D., Cook, M.S., 2010. Last glacial maximum to Holocene sea surface conditions at Umnak Plateau, Bering Sea, as inferred from diatom, alkenone, and stable isotope records. Paleoceanography 25, PA1206. http://dx.doi.org/10.1029/2008PA001671.

Clark, P.U., Archer, D., Pollard, D., Blum, J.D., Rial, J.A., Brovkin, V., Mix, A.C., Pisias, N.G., Roy, M., 2006. The Middle Pleistocene Transition: characteristics, mechanisms, and implications for long-term changes in atmospheric pCO_2. Quaternary Science Reviews 25, 3150–3184.

Clement, J.L., Maslowski, W., Cooper, L.W., Grebmeier, J.M., Walczowski, W., 2005. Ocean circulation and exchange through the northern Bering Sea—1979–2001 model results. Deep-Sea Research Part II 52, 3509–3540.

Crundwell, M., Scott, G., Naish, T., Carter, L., 2008. Glacial–interglacial ocean climate variability from planktonic foraminifera during the Mid-Pleistocene Transition in the temperate Southwest Pacific, ODP Site 1123. Palaeogeography, Palaeoclimatology, Palaeoecology 260, 202–229.

de Garidel-Thoron, T., Rosenthal, Y., Bassinot, F., Beaufort, L., 2005. Stable sea surface temperatures in the western Pacific warm pool over the past 1.75 million years. Nature 433, 294–298.

DeMaster, D.J., 1981. The supply and accumulation of silica in the marine environment. Geochimica et Cosmochimica Acta 5, 1715–1732.

Expedition 323 Scientists, 2009. Bering Sea paleoceanography: Pliocene–Pleistocene paleoceanography and climate history of the Bering Sea. IODP Prel. Rept., 323. http://dx.doi.org/10.2204/iodp.pr.323.2009.

Haug, G.H., Maslin, M.A., Sarnthein, M., Stax, R., Tiedemann, 1995. Evolution of northwest Pacific sedimentation patterns since 6 Ma (Site 882). In: Rea, D.K., Basov, I.A., Scholl, D.W., Allan, J.F. (Eds.), Proc. ODP Sci. Results, 145. Ocean Drilling Program, College Station, TX, pp. 293–314.

Haug, G.H., Sigman, D.M., Tiedemann, R., Pedersen, T.F., Sarnthein, M., 1999. Onset of permanent stratification in the subarctic Pacific Ocean. Nature 401, 779–782.

Imbrie, J.Z., Imbrie-Moore, A., Lisiecki, L.E., 2011. A phase-space model for Pleistocene ice volume. Earth and Planetary Science Letters 307, 94–102.

Itaki, T., Uchida, M., Kim, S., Shin, H.S., Tada, R., Khim, B.K., 2009. Late Pleistocene stratigraphy and paleoceanographic implications in northern Bering Sea slope sediments: evidence from the radiolarian species *Cycladophora davisiana*. Journal of Quaternary Science 24, 856–865.

Iwasaki, S., Takahashi, K., Kanematsu, Y., Sakamoto, T., Sakai, S., Onodera, J., Asahi, H., Ravelo, A.C., Science Team of IODP Exp. 323, 2011. Paleoproductivity and paleoceanography of the last 4.3 Myrs at IODP Exp. 323 Site U1341 in the Bering Sea based on biogenic opal content. American Geophysical Union, Fall Meeting, abstract #PP31B-1865.

Kanematsu, Y., Takahashi, K., Kim, S., Khim, B.K., Asahi, H., 2013. Changes in biogenic opal productivity with Milankovitch cycle during the last 1.3 Myrs at IODP Expedition 323 Sites U1341, U1343, and U1345 in the Bering Sea. Quaternary International 310, 213–220.

Kim, S., Khim, B.K., Takahashi, K., IODP Expedition 323 Scientists, 2010. High-resolution variation of biogenic opal content in the Bering Sea (IODP Expedition 323, Site U1343) from the late Pliocene to early Pleistocene (2.2 Ma to 1.4 Ma). American Geophysical Union, Fall Meeting, abstract #PP21B-1695.

Kim, S., Khim, B.K., Uchida, M., Tada, R., 2011. Millennial-scale paleoceanographic events and implication for the intermediate-water ventilation in the northern slope area of the Bering Sea during the last 71 kyrs. Global and Planetary Change 79, 89–98.

Kitamura, A., Kawagoe, T., 2006. Eustatic sea-level change at the Mid-Pleistocene climate transition: new evidence from the shallow-marine sediment record of Japan. Quaternary Science Reviews 25, 323–335.

Lisiecki, L.E., Raymo, M.E., 2005. A Pliocene–Pleistocene stack of 57 globally distributed benthic $\delta^{18}O$ records. Paleoceanography 20, PA1003. http://dx.doi.org/10.1029/2004PA001071.

Liu, Z., Herbert, T.D., 2004. High-latitude influence on the eastern equatorial Pacific climate in the early Pleistocene epoch. Nature 427, 720–723.

Marino, M., Maiorano, P., Lirer, F., 2008. Changes in calcareous nannofossil assemblages during the Mid-Pleistocene Revolution. Marine Micropaleontology 69, 70–90.

Martinez-Garcia, A., Rosell-Mele, A., McClymont, E.L., Gersonde, R., Haug, G.H., 2010. Subpolar link to the emergence of the modern equatorial Pacific cold tongue. Science 328, 1550–1553.

McClymont, E.L., Rossel-Mele, A., 2005. Links between the onset of modern Walker circulation and the mid-Pleistocene climate transition. Geology 33, 389–392.

McClymont, E.L., Rosell-Mele, A., Haug, G., Lloyd, J., 2008. Expansion of subarctic water masses in the North Atlantic and Pacific oceans and implications for mid-Pleistocene ice sheet growth. Paleoceanography 23, PA4214. http://dx.doi.org/10.1029/2008PA001622.

Mortlock, R.A., Rroelich, P.N., 1989. A simple method for the rapid determination of opal in pelagic marine sediments. Deep-Sea Research 36, 1415–1426.

Mudelsee, M., Raymo, M.E., 2005. Slow dynamics of the Northern Hemisphere glaciation. Paleoceanography 20, PA4022. http://dx.doi.org/10.1029/2005PA001153.

Nakatsuka, T., Watanabe, K., Handa, N., Matsumoto, E., Wada, E., 1995. Glacial to interglacial surface nutrient variations of Bering deep basins recorded by $\delta^{13}C$ and $\delta^{15}N$ of sedimentary organic matter. Paleoceanography 10, 1047–1061.

Okazaki, Y., Takahashi, K., Asahi, H., Katsuki, K., Hori, J., Yasuda, H., Sagawa, Y., Tokuyama, H., 2005. Productivity changes in the Bering Sea during the late Quaternary. Deep-Sea Research Part II 52, 2150–2162.

Okkonen, S.R., Schmidt, G.M., Cokelet, E.D., Stabeno, P.J., 2004. Satellite and hydrographic observations of the Bering Sea 'Green Belt'. Deep-Sea Research Part II 51, 1033–1051.

Raymo, M.E., Oppo, D.W., Curry, W., 1997. The mid-Pleistocene climate transition: a deep sea carbon isotopic perspective. Paleoceanography 12, 546–559.

Rea, D.K., Snoeckx, H., 1995. Sediment fluxes in the Gulf of Alaska: paleoceanographic record from Site 887 on the Patton-Murray seamount platform. In: Rea, D.K., Basov, I.A., Scholl, D.W., Allan, J.F. (Eds.), Proc. ODP Sci. Results, 145. Ocean Drilling Program, College Station, TX, pp. 247–256.

Schefus, E., Sinninghe Damste, J.S.S., Jansen, J.H.F., 2004. Forcing of tropical Atlantic sea surface temperatures during the mid-Pleistocene transition. Paleoceanography 19, PA4029. http://dx.doi.org/10.1029/2003PA000892.

Shackleton, N.J., Hall, M.A., 1989. Stable isotope history of the Pleistocene at ODP Site 677. In: Becker, K., Sakai, H., et al. (Eds.), Proc. ODP Sci. Results, 111. Ocean Drilling Program, College Station, TX, pp. 295–316.

Shackleton, N.J., Imbrie, J., Pisias, N.G., 1988. The evolution of oceanic oxygen-isotope variability in the North Atlantic over the past 3 million years. Philosophical Transactions of the Royal Society of London. Series B, Biological Sciences 318, 679–686.

Snoeckx, H., Rea, D.K., Jones, C.E., Ingram, B.L., 1995. Eolian and silica deposition in the central North Pacific: results from Sites 885/886. In: Rea, D.K., Basov, I.A., Scholl, D.W., Allan, J.F. (Eds.), Proc. ODP Sci. Results, 145. Ocean Drilling Program, College Station, TX, pp. 219–230.

Sorokin, Y.I., 1999. Data on primary production in the Bering Sea and adjacent Northern Pacific. Journal of Plankton Research 32, 615–636.

Springer, A.M., McRoy, P.C., Flint, M.V., 1996. The Bering Sea Green Belt: shelf-edge processes and ecosystem production. Fisheries Oceanography 5, 205–223.

St. John, K.E.K., Krissek, L.A., 1999. Regional patterns of Pleistocene ice-rafted debris flux in the North Pacific. Paleoceanography 14 (5), 653–662. http://dx.doi.org/10.1029/1999PA900030.

Stabeno, P.J., Bond, N.A., Hermann, A.J., Kachel, N.B., Mordy, C.W., Overland, J.E., 2004. Mateorology and oceanography of the northern Gulf of Alaska. Continental Shelf Research 24, 859–897. http://dx.doi.org/10.1016/j.csr.2004.02.007.

Takahashi, K., Ravelo, A.C., Zarikian, C.A., IODP Expedition 323 Scientists, 2011. IODP Expedition 323—Pliocene and Pleistocene paleoceanographic changes in the Bering Sea. Scientific Drilling 11, 4–13. http://dx.doi.org/10.2204/iodp.sd.11.01.2011.

Teraishi, A., Suto, I., Onodera, J., Takahashi, K., 2013. Diatom, silicoflagellate and ebridian biostratigraphy and paleoceanography in IODP 323 Hole U1343E at the Bering slope site. Deep-Sea Research Part II (in press).

Tsuda, A., Kiyosawa, H., Kuwata, A., Mochizuki, M., Shiga, N., Saito, H., Chiba, S., Imai, K., Nishioka, J., Ono, T., 2005. Responses of diatoms to iron-enrichment (SEEDS) in the western subarctic Pacific, temporal and special comparisons. Progress in Oceanography 64, 189–205. http://dx.doi.org/10.1016/j.pocean.2005.02.008.

https://doi.org/10.1016/j.yqres.2013.10.001 Published online by Cambridge University Press